Numerical Investigation of Atherosclerotic Plaque Rupture using Optical Coherence Tomography Imaging and XFEM

Phani Kumari Paritala
School of Chemistry, Physics and Mechanical Engineering
Queensland University of Technology,
Brisbane 4000, Australia
phanikumari.paritala@hdr.qut.edu.au

Prasad KDV Yarlagadda
School of Chemistry, Physics and Mechanical Engineering
Queensland University of Technology,
Brisbane 4000, Australia
y.prasad@qut.edu.au

Jiaqiu Wang
School of Chemistry, Physics and Mechanical Engineering
Queensland University of Technology,
Brisbane 4000, Australia
jiaqiu.wang@hdr.qut.edu.au

YuanTong Gu
School of Chemistry, Physics and Mechanical Engineering
Queensland University of Technology,
Brisbane 4000, Australia
yuantong.gu@qut.edu.au

Zhiyong Li[1]
School of Chemistry, Physics and Mechanical Engineering
Queensland University of Technology,
Brisbane 4000, Australia
zhiyong.li@qut.edu.au

ABSTRACT

Myocardial infarction contributes to most fatalities in which atherosclerotic plaque disruption is the underlying pathology. From the mechanics view point, the pulsatile blood flow in the arteries resembles a fatigue environment and generates stresses that affect the rupture of the atherosclerotic plaque. In this context, patient-specific optical coherence tomography (OCT) was used to develop the fatigue crack growth behavior. The impact of location specific morphological features and their relative effect on plaque life were discussed. EXtended Finite Element Method (XFEM) and Paris' Law were employed to investigate the fatigue crack growth. Twelve 2D slices from six patients were reconstructed for studying the fatigue crack growth behavior. Our results indicate that plaque life decreases with an increase in pulse pressure and 53.5% of the total cracks initiated at various locations on the lumen lead to rupture. 73.7% of the rupture locations did not have calcifications. Correlation between the location specific morphology and the rupture indicates that for a 1 mm increase in the fibrous cap thickness there is a large decrease in the odds of rupture [0.163 (0.073; 0.363)], p-value < 0.0001; and for a 1 mm^2 increase of the calcification area, there is a decrease in the odds of rupture by 0.719 (0.619; 0.835), p-value <0.0001. In conclusion, the XFEM technique can be used to study the fatigue behavior of the atherosclerotic plaque that depends on the combined effects of plaque constituents and their morphology. It may help to better assess plaque vulnerability and make more accurate predictions for plaque rupture.

[1] Zhiyong Li, Email: zhiyong.li@qut.edu.au

School of Chemistry, Physics and Mechanical Engineering, Queensland University of Technology, Brisbane 4000, Australia.

1. INTRODUCTION

Cardiovascular diseases (CVD), the leading causes of morbidity and mortality globally are accounting for approximately 43,602 deaths in Australia [1] and 1 in every 3 deaths in the United States [2] and are projected to increase over the next few years [3]. Atherosclerotic plaque rupture is a significant cause for the majority of the cardiovascular events with a major share contributed to myocardial infarction [3]. Plaque initiation, progression, and rupture are complex processes. Several factors such as mechanical forces, plaque morphology, blood conditions, hypertension, living and eating habits influence the process. Plaque rupture occurs when stress, acting on the lesion, is greater than the strength. An atherosclerotic plaque rupture is a catastrophic event which depends on the plaque composition and vulnerability [4]. Vulnerable plaques often have thin fibrous caps and are susceptible to rupture leading to the thrombus. Unstable plaques vulnerable to rupture are characterized by a thin fibrous cap and inflammation, calcification, and intraplaque hemorrhage [5, 6]. Various histological studies of the atherosclerotic plaque have shown that the main reason for the majority of coronary events is the formation of thrombosis, due to plaque fissuring [7], and the indicators for high-risk plaque were found to be a large necrotic core with a very thin fibrous cap called thin cap fibroatheroma (TCFA) [8], calcified and stenotic lesions [9-11].

Luminal stenosis is the main feature assessed by traditional angiographic techniques. However, many of the culprit lesions causing acute cardiovascular events are not highly stenotic, because the artery undergoes positive remodeling well before the plaque encroaches into the lumen [12]. Moreover, plaque composition is rather more important than plaque size and is responsible for the cardiovascular events. The biomechanical assessment of the plaque rupture is well-thought-out as a structural event that happens when the stress acting on the lesion is greater than the strength. Therefore, to study the biomechanics of atherosclerotic plaque rupture, various techniques and models including 2D & 3D idealized and patient specific models of carotid and coronary arteries were used by different research groups for performing different analysis such as

structural only, fluid structure interaction and fatigue [4, 13-19]. It was found that the pulsatile blood flow in the arteries exerts mechanical forces on the vessel wall, generating mechanical stresses that affect the initiation, progression, and rupture of the atherosclerotic plaque[20]. Alterations in the wall shear stresses (WSS) are responsible for the initiation and progression of the plaque whereas the plaque structural stresses (PSS) are responsible for the rupture of the vulnerable plaque [21]. Also, a moderate stenosis with a thin fibrous cap indicated a high risk of plaque rupture[22].

Bank et al. [23] hypothesized fatigue as a critical biomechanical mechanism underlying atherosclerotic plaque rupture. The cardiovascular system resembling a fatigue environment under the systole and diastole phases of the cardiac cycle at a heart rate of 70 beats per minute, refers to a recurring failure induced by cyclic loading resulting in a catastrophic event. Fatigue failure is the accumulation of the damage due to repeated loading that occurs at points of stress concentration where the stresses are much lower than those needed to rupture the plaque with monotonic tension. Our group has previously developed idealized two-dimensional models to quantify the fatigue life of the atherosclerotic plaque and also studied the effect of calcification on the vulnerability [24, 25]. Also a rupture risk index was defined to study the difference between symptomatic and asymptomatic patients [19, 26]. Earlier studies that focused on two-dimensional models by using the most conservative biomechanical concept investigated the impact of anatomy, tissue properties, and blood pressure on the fatigue mechanism [27]. In vivo, MRI-based patient-specific imaging data of 27 patients with carotid artery disease explained the development of cracks in fibrous cap, which ultimately lead to rupture and matched with the locations of in vivo observed fibrous cap defects [28]. Histology-based reconstructed models showed that the secondary cracks initiated at the shoulder regions may be more critical than the initial cracks [29].

However, lack of accurate patient-specific models of the atherosclerotic plaque rupture and the difficulty of updating the mesh in order to track the crack path were among limitations of the previous studies. Moreover, no attention has been paid to the critical locations on the lumen apart from the maximum stress location. Accordingly, the

objective of this study is to further investigate the fatigue process at various locations on the lumen using optical coherence tomography (OCT) imaging, which has a high resolution and is better for the characterization of the fibrous cap. In addition, a numerical method eXtended Finite Element Method (XFEM) is used for modeling the crack growth which eliminates the need to remesh the discontinuity in every step of the simulation thereby reducing the computation costs and errors associated with conventional methods. Furthermore, developing a statistical correlation of the fatigue life of the plaque (rupture and unrupture) with the morphology at the crack sites and investigate the relative significance of morphological features for the risk assessment.

2. MATERIALS AND METHODS

The 2D finite element models of the atherosclerotic plaque used for fatigue crack growth modeling were reconstructed from the OCT imaging data obtained from the Prince Charles Hospital. A human low-risk ethics approval (approval number: 1500000308) has been obtained for this study. Twelve different geometries of varying morphology and constituents were reconstructed from six different patients to study the effect of the morphology and constituents on the fatigue life and the vulnerability of the plaque.

2.1 Geometry Reconstruction

The OCT data of six patients was used to reconstruct twelve patient-specific 2D slices containing calcification and/or lipid core. The raw data which is in polar coordinates contain a series of slices of the patient imaging data of the region of interest as shown in Fig 1(a). Initially, a MATLAB (version 2017a, Mathworks, Natick, MA, US) program was employed to convert the coordinates of the data from polar to orthogonal so that a section view of the artery as shown in Fig. 1(b) was visible. Then these slices were processed by adjusting contrast and brightness by an open source software ImageJ (imagej.nih.gov/ij/) Fig (c). The manual segmentation of processed slices was done in

ImageJ following the appearance illustrated in Table 1 [30] to get the x and y coordinates of the respective constituents. The coordinates were saved as a .txt file in the format required for a finite element solver. The text files were imported to Ansys as a curve that is created from the co-ordinates file and later the surfaces were generated from the edges. Fig.1 shows the geometry reconstruction process from the patient-specific slices.

Table 1. Image Characteristics of Optical Coherence Tomography

Tissue type	Image characteristics
Normal Vessel wall	Dark band of muscular media, delimited by internal elastic lamina and external elastic lamina
Fibrous tissue	Homogeneous, high reflectivity and low attenuation
Calcification	Sharp edges, low reflectivity, and low attenuation
Lipid	Diffuse edges, high reflectivity, and high attenuation
Red thrombus	Medium reflectivity and high attenuation
White thrombus	Medium reflectivity and low attenuation

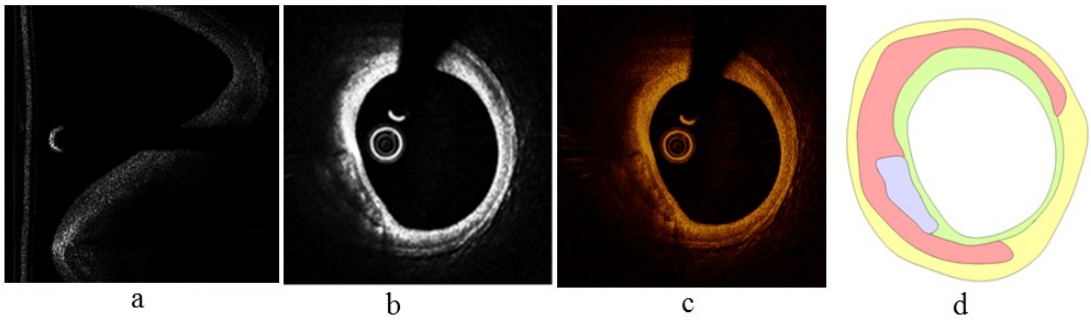

Fig. 1. Reconstruction of patient specific geometry, **a:** Raw OCT data (polar coordinates), **b:** Grey scale image (orthogonal coordinates), **c:** False colour image (orthogonal Coordinates), **d:** The reconstructed 2D geometry.

2.2 Modeling

In view of the fact that the cardiovascular system resembles a fatigue environment under repeated systole and diastole phases, the biomechanical analysis of the plaque rupture seems to be a useful tool to investigate the fatigue life of the plaque. The fatigue failure of the plaque under pulsatile environment also requires more insight and research for assessing the plaque vulnerability. Thereby, the concepts of fracture mechanics were

used to predict the fatigue life of the atherosclerotic plaque. The eXtended Finite Element Method was used to simulate the fatigue crack growth and Ansys (version 18.0, ANSYS Inc., Canonsburg, PA, US) was used for the simulations.

2.2.1 Fracture Mechanics

In this study, stress intensity factor (K) that describes the stress state at a crack tip was used to establish failure criteria and material properties were defined as linear elastic. For, isotropic linear elastic material properties the stress field ahead of the crack tip was proportional to $1 \sqrt{r}$ and was expressed as $\sigma ij = (K \sqrt{2\pi r}) fij(\theta)$ [31]. Paris' Law [32] was used to determine the fatigue crack growth. According to Paris, fatigue crack growth rate depends on the stress intensity factor and is expressed as

$$\frac{da}{dN} = C.(\Delta K)^m \qquad (1)$$

Where $\frac{da}{dN}$ is crack extension per cycle of load, ΔK is stress intensity factor range. C, and m are material constants and C=1, m=2.6 were chosen as suggested by previous studies [24, 25]. The stress intensity factor was evaluated by the interaction integral method that applies area integration for 2D problems and offers a better accuracy. The maximum circumferential stress criteria [33] was adopted to calculate the crack propagation direction and is given by θ in equation 2, where K_I and K_{II} are stress intensity factors. Based on this theory, the crack propagates in a radial direction on the plane perpendicular to the normal stress [34].

$$\theta = \cos^{-1} \frac{3(K_I)_{max} + (K_I)_{max} \sqrt{(K_I)^2{}_{max} + 8(K_{II})^2{}_{max}}}{(K_I)^2{}_{max} + 9(K_{II})^2{}_{max}} \qquad (2)$$

2.2.2 Extended Finite Element Method

The eXtended Finite Element Method (XFEM) [35], based on the partition of unity method [36] was used to model the fatigue crack growth simulations. In this method, the crack can be modeled independently of finite element mesh thereby eliminating the need of updating the mesh near the crack-tip region at every step as in the standard finite

element method. XFEM extends the standard FE formulation by incorporating additional enrichment functions which account for crack-tip singularities (asymptotic crack tip functions) and jumps in displacements across the crack surfaces (Heaviside jump functions). The displacement vector is given by

$$u(x) = N_I(x)u_I + H(x)N_I(x)a_I + N_I(x)\sum_j F_j(x)b_I^j \qquad (3)$$

Where

$u(x)$ = displacement vector,

$N_I(x)$ = nodal shape functions,

u_I = nodal displacement vector,

$H(x)$ = Heaviside jump function,

a_I = enriched nodal degree of freedom,

$F_j(x)$= asymptotic crack tip functions,

b_I^j = nodal degrees of freedom.

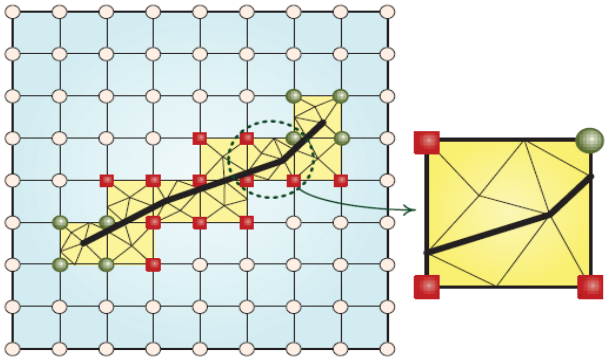

Fig. 2. Numerical integration of the discontinuity based on triangular subdivisions

The numerical integration of the discontinuity was based on the triangular subdivisions at the crack tip as shown in Fig. 2 [34]. Heaviside step functions were used to enrich the nodal points of the elements cut by the crack represented by squared points and asymptotic functions were used to enrich the nodal points at the crack tip represented by circled points. The stress and displacement fields were evaluated based on the enrichment functions and the new crack tip position was identified. Level set method [37] was used to track and determine the moving crack location in the model. The length of

the crack propagated in every step was defined by the length of the element ahead of the crack tip. Figure 3 shows the initial crack location on a 2D slice based on the maximum circumferential stress criteria and the independent meshing based on the extended finite element method.

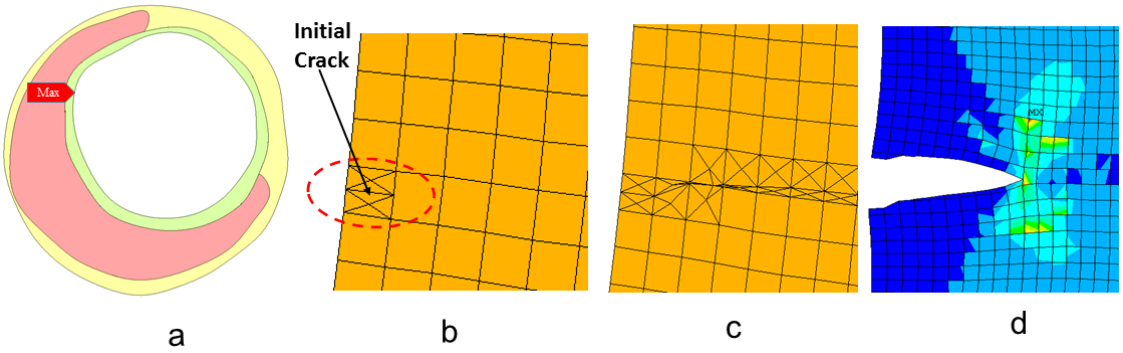

Fig. 3. Initial crack location and meshing. **a:** Maximum circumferential stress location, **b:** Initial crack and numerical integration of discontinuity, **c:** Independent meshing as the crack propagates, **d:** Crack opening

2.2.3 Fatigue Crack Growth Modeling

Twelve different slices of varying morphology shown in Fig. 4 were reconstructed from the OCT imaging data of the coronary artery. Plane 182 elements with linear elastic isotropic material properties and plane strain behavior were used for the analysis. Mesh sensitivity analysis (Fig. 5) was performed varying the mesh size with all other parameters constant. The mesh size of 0.0075 mm around the crack tip and 0.025 mm for the rest of the geometry were selected to avoid the variation of results based on the balance between mesh sensitivity and computation cost. An elastic support was defined on the outer wall of the artery assuming that the coronary artery is surrounded by a soft connective tissue. The stiffness of 0.0005 N/mm^3 was chosen based on the sensitivity analysis performed by changing the stiffness values with all other parameters constant as shown in Fig. 5. A uniformly distributed pressure load of 120 mmHg (systolic pressure) was defined on the lumen. Based on the concepts of fracture mechanics, the crack was initiated at the maximum stress location. Therefore, for the first set of simulations, the maximum stress location on the lumen was defined as the initial crack and the pulse

pressure (systolic pressure - diastolic pressure) was increased to study the effect of pressure on the fatigue life of the plaque as shown in Table 2.

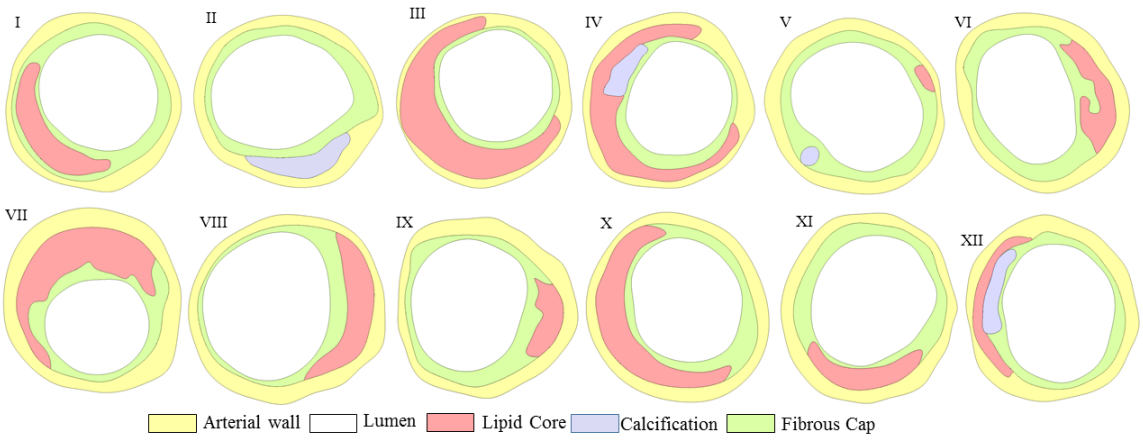

Fig. 4. The reconstructed 2D models based on OCT imaging data

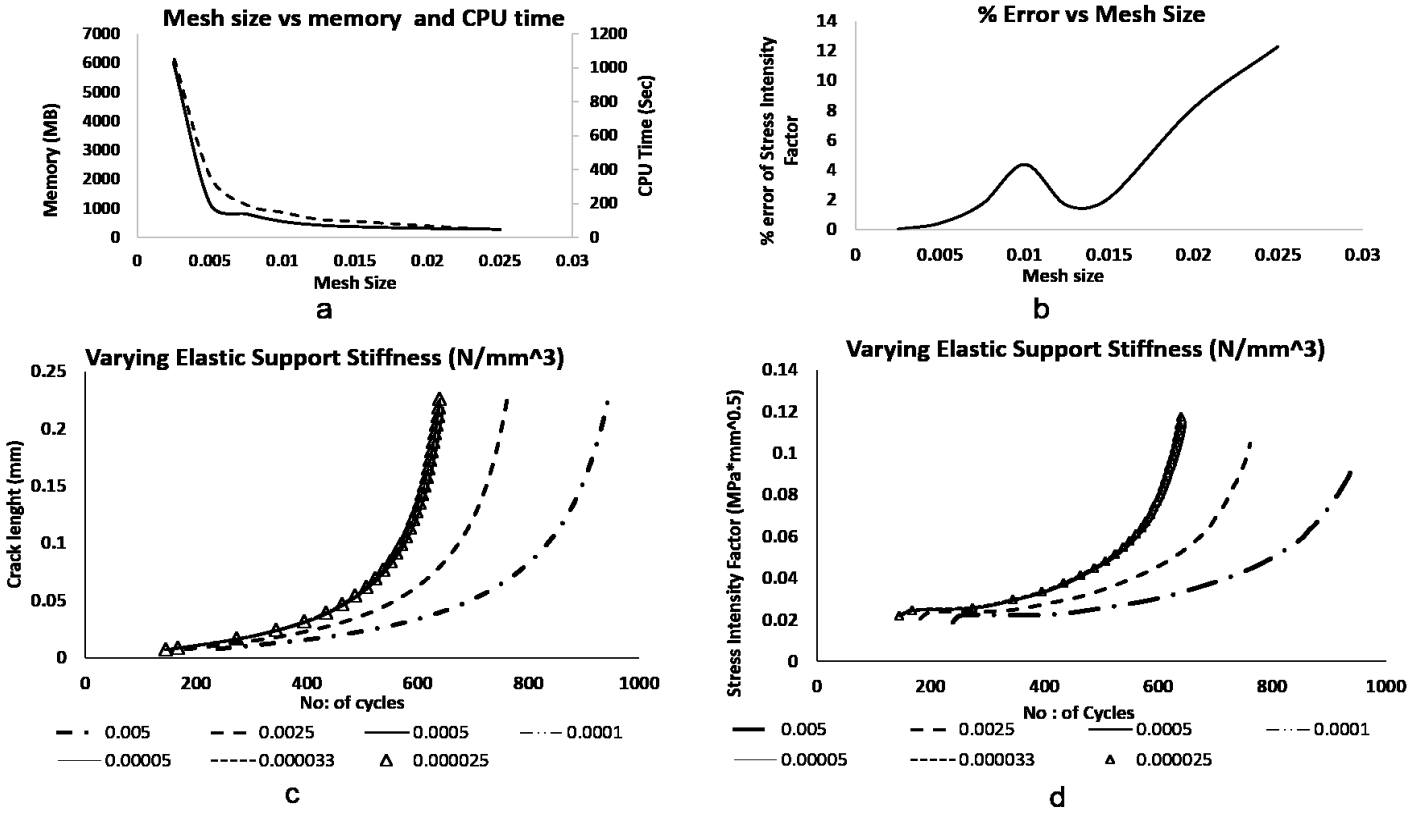

Fig. 5. Sensitivity analysis. **a:** Mesh size vs memory and CPU time, **b:** % Error vs mesh size, **c:** Number of cycles vs crack length, **d:** Number of cycles vs stress intensity factor

Table 2. Input parameters for the simulations

Set	Systolic Pressure (SP) mmHg	Diastolic Pressure (DP) mmHg	Pulse Pressure (PP) mmHg	Stress Ratio DP/SP	Initial crack location	No. of simulations
1	120	80	40	0.67	Maximum Stress Location	1
	160	107	53			1
	200	134	66			1
2	120	80	40		MSL & interval of 20^0 on lumen	19

Later, in the second set of simulations, a cyclic loading of a constant amplitude (80-120 mmHg) was defined on the lumen. To study the effect of morphology, and constituents on fatigue life of the plaque, various crack initiation locations were defined on the lumen at an interval of 20^o anticlockwise, starting from the positive x-axis. The stress ratio was kept constant for all the simulations. The crack tip, coordinate system at the crack tip, Paris law constants, enrichment region, and singularity radius were also defined. The material properties were assumed to be linear elastic as listed in Table 3 and Paris law constants were chosen as C=1, m=2.6 as suggested by previous studies [24, 25]. Please note that due to the lack of experimental measurements of C and m values, they were adopted from the literature. An initial crack of length 0.0075 mm was defined and the crack increment for every step was defined by the length of the element ahead of the crack tip. The number of incremental cycles was calculated by the fatigue crack growth law. The morphological features such as location-specific fibrous cap thickness (FCT), lipid core thickness (LCT) and slice specific lipid core area (LCA), fibrous cap area (FCA), calcification area (CA) were measured from the models.

Table 3. Material properties of different constituents of the atherosclerotic plaque

Component	Young's Modulus E (MPa)	Poisson's Ratio ν
Arterial wall	E_{aw} = 0.3	0.48
Fibrous cap	E_{fc} = 0.6	0.48
Lipid core	E_{lp} = 0.02	0.48
Calcification	E_{cal} = 10	0.48

2.3 Statistical Analysis

Data analysis was performed using SPSS (version 23.0), $p < 0.05$ was established the level of statistical significance. Descriptive statistics were used to describe the baseline features of the data in the study and any correlations of the variables between groups (rupture and unrupture) were studied. Generalized estimating equations (GEE), an extension of the generalized linear models (GLM) which provided a framework for analyzing the correlated data from repeated measures was used for the analysis of the data related to the second set of simulations [38]. A binary logistic model was used to explore the correlations between various morphological features (FCT, LCT, LCA, CA, and Calcification) and the plaque rupture. Backward elimination method was used for finding the best predictive model. Initially, all the variables of interest were put in the model followed by eliminating one variable at a time if they did not contribute to the regression coefficient. The changes in the estimated logistic regression coefficients (crude vs adjusted) were studied.

3. RESULTS

In total 12 OCT slices (4 with calcification) were used to study the effect of blood pressure, morphology, constituents, and location of the crack initiation point on plaque fatigue life. Following the basic concepts of fatigue, an initial crack and then crack tip were defined on the lumen at the location of the maximum circumferential stress. Also, singularity enrichment region and enhancement radius were defined to include the singularity functions to account for the crack tip singularity around the crack tip [39].

For the first set of simulations on 12 slices shown in Fig. 3, the pulse pressure was set at 40, 53, and 66 mmHg. The stress ratio was set constant as shown in Table 2. Cracks extended radially and the crack growth rate increased with the increase in pulse pressure thereby decreasing the plaque life, see Fig. 7(a). For, the second set of simulation, the cracks were initiated at 18 different locations on the lumen surface at an interval of 20°

each. Fig. 6 shows a typical crack initiation location for slice III. The plaque life of all the 12 slices at 18 different locations were shown in Fig. 7(b) indicated that 53.5% of the total cracks initiated including the maximum circumferential stress location lead to rupture [27]. While 73.7% of the locations at which the crack has propagated and lead to rupture did not have calcification. The reason for unrupture at different locations depended upon the morphology and constituents present at that location [21].

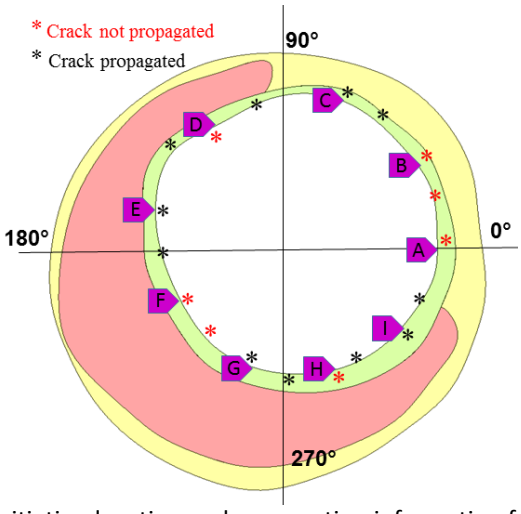

Fig. 6. A typical crack initiation location and propagation information for slice III

In Fig. 8(a), it is observed that the compressive stresses were acting ahead of the crack at the initial stage or during the crack propagation thereby resulting in crack closure rather than opening. At various locations based on the constituents ahead of the crack tip, compressive stresses were found to act thereby resulting in crack closure rather than opening, see Fig. 8(b)[29]. The compressive stresses found at the initial stage may reduce the chance of crack initiation at that location. Also, the compressive stresses acting at the crack tip during the crack propagation opposed the crack from growing further. This phenomenon is called crack arrest in fracture mechanics [40].

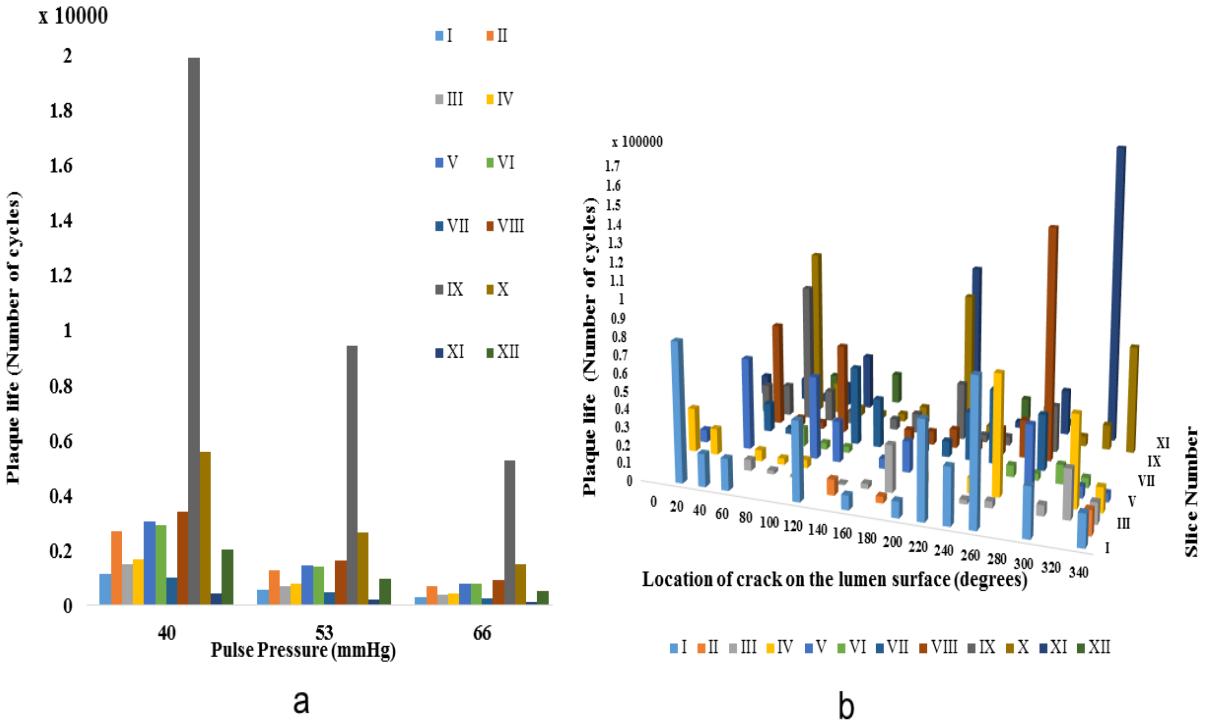

Fig. 7. Plaque Life, **a:** Variation of plaque fatigue life with changes in pulse pressure **b:** Plaque fatigue life of cracks initiated at different locations on the lumen surface on respective slices

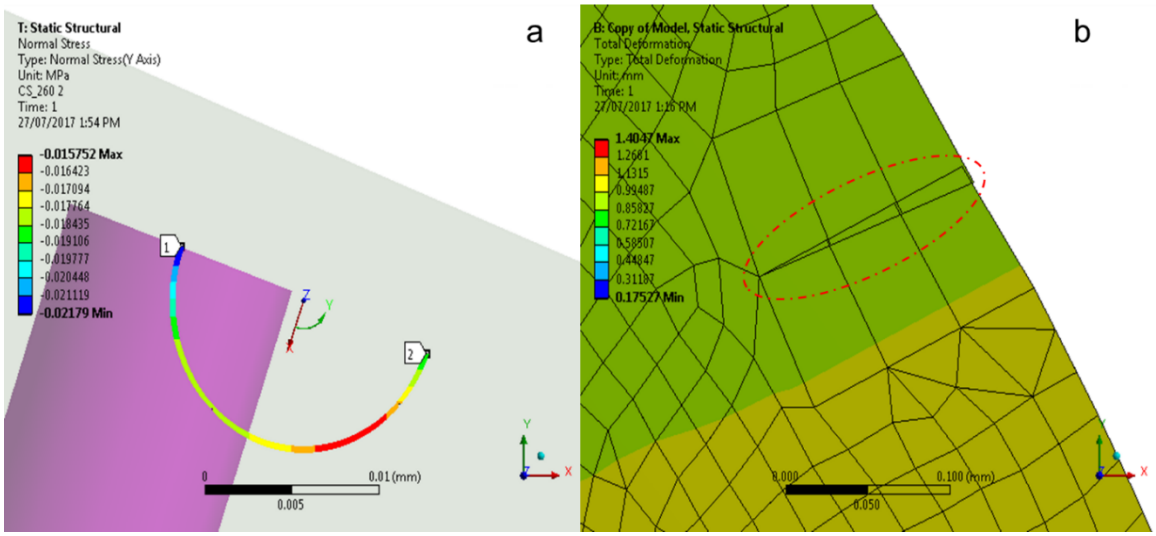

Fig. 8. Stresses acting at the crack tip, **a** Compressive stresses at the crack tip, **b** Right: Crack closing due to compressive stresses

The distribution of the FCT and LCA for rupture and unrupture cases based on the statistical analysis are illustrated in Fig. 9 as they are the crucial characteristics of vulnerable plaque [41]. The boxes encompass the interquartile range that describes the middle 50% of the values and the horizontal line in the boxes represent the median values. The upper and the lower whiskers represent the 75th percentile and 25th percentile values with the exception of outliers (1.5 times the interquartile range) represented by hollow circles. Fig. 9(a), reveals that the median of FCT is lower for rupture than unrupture group, explaining the influence of FCT on the plaque vulnerability. Unlike FCT the median of LPA is more for the ruptured locations compared to unruptured locations as shown in Fig 9(b). The results of the GEE analysis, showing associations between morphological features, were presented in Table 4. The logistic regression coefficients indicate that for 1 mm increase in fibrous cap thickness there was a large decrease in the odds of rupture [0.163 (0.073; 0.363)] and is statistically significant with a p-value < 0.0001, and 1 mm^2 increase in lipid core area corresponds to an increase in the odds of rupture by 2.1% [1.021 ((0.999; 1.044)]. Also, for 1 mm^2 increase of the calcification area, there is a decrease in the odds of rupture by 0.719 (0.619; 0.835) and is statistically significant with a p-value <0.0001.

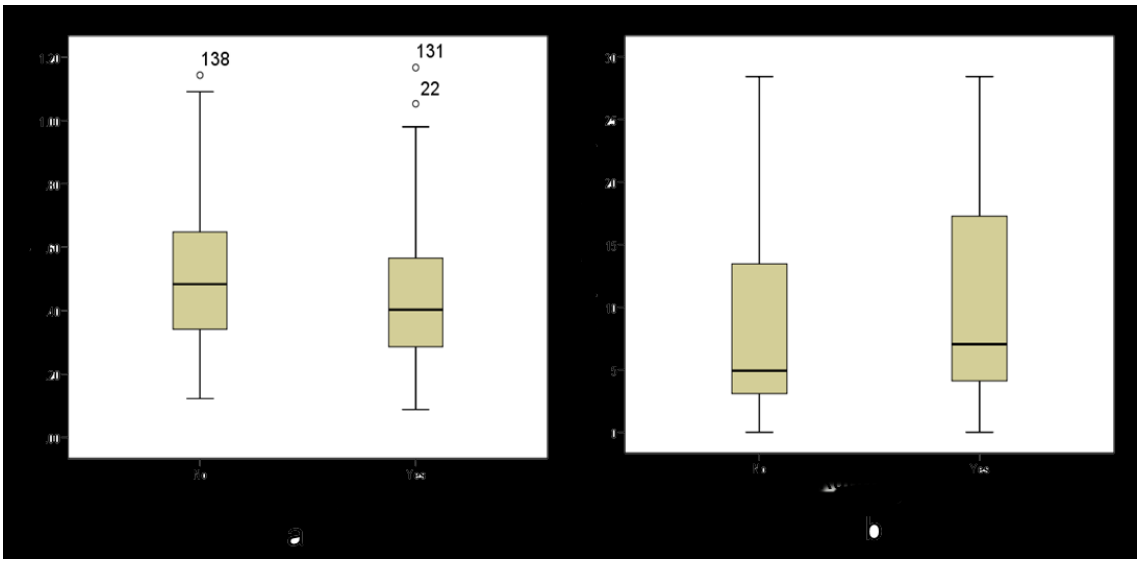

Fig. 9. Box plots, **a:** Comparison of local fibrous cap thickness for the rupture and the unrupture groups, **b:** Comparison of lipid core area for the rupture and the unrupture groups

Table 4 Association between various morphological features

	Crude Model		P-value	Adjusted Model		P-value
	Odds	95% Confidence interval for Odds		Odds	95% Confidence interval for Odds	
FCT	0.189	(0.065; 0.552)	0.002	0.163	(0.073; 0.363)	< 0.0001
LCA	1.033	(0.996; 1.070)	0.080	1.021	(0.999; 1.044)	0.064
CA	0.787	(0.660; 0.938)	0.007	0.719	(0.619; 0.835)	< 0.0001
Calcification(Y/N)	0.501	(0.249; 1.006)	0.052	1.687	(0.979; 2.906)	0.060
LCT	0.829	(0.463; 1.483)	0.527			
FCA	0.967	(0.885; 1.057)	0.458			

4. DISCUSSION

To best of our knowledge, this is the first study to explore fatigue life of the plaque using in-vivo OCT based patient specific data and XFEM. Most investigations studied the fatigue process of the atherosclerotic plaque rupture using idealized models and patient specific MRI or histology based models [23, 24, 28, 29]. Also, the computational cost and errors associated with conventional methods were overcome by using XFEM. Earlier patient-specific studies focused on the effect of blood pressure and the maximum stress location for crack initiation. But, the present study used high resolution OCT-based reconstructed models, and investigated the fatigue crack growth at various locations on the lumen following our group's work that showed the maximum stress location was not the only critical location which has a minimum fatigue life. In addition, statistical correlations of the location specific morphological features with plaque life were identified for better understanding the cumulative effect of all the constituents present at that location.

Rupture of the fibrous cap being a biomechanical event and several factors such as mechanical forces, plaque morphology, and blood pressure, living and eating habits influence the process. The crack initiation location is very critical for the stability of the

plaque. Therefore, the fatigue crack growth behavior was studied at 19 different locations including the maximum stress location. The numerical results suggest that morphological features and constituents affect the plaque stability. Also, a decrease in heart rate and pulse pressure can lead to an increase in the stability of the atherosclerotic plaque.

From the results, it was observed that cracks were initiated at the location of the maximum stress along the lumen surface and did not change with a change in pulse pressure [27] in relation to the findings that plaque was most vulnerable at the regions of stress concentration [42]. In accordance with [24], it was also found that cracks initiated at the maximum stress location may not be the critical location for the failure of the plaque as the fatigue life depended upon the morphological features at the particular location of interest. Also, the functioning and disease progression in the arteries is a combination of systemic, hemodynamic and biological factors [43] the crack can be initiated in any location based on components and patient specific risk factors. Plaque life being sensitive to the variations in local morphological features, the morphology of plaque constituents at all the crack initiation locations were measured from the reconstructed models. The distribution of the FCT and LCA for rupture and unrupture cases were studied and the fibrous cap thickness at the crack initiation location remains the crucial feature in the assessment of plaque vulnerability which is statistically significant ($P<0.0001$) [8, 44, 45]. It was observed that decrease in fibrous cap thickness and increase in lipid core area, decreased the plaque life [46]. Calcification affected plaque stability. Large deposits of calcium increased the plaque stability ($p<0.0001$) and the presence/ absence of calcification in the slices had a profound effect on the plaque life. It was observed that rapid changes in the stress values at the crack tip in the plaque and the calcification region were very important and they may be the critical factors for plaque life.

Although this study has successfully demonstrated the effect of blood pressure and the plaque morphological features on the stability of the plaque, it has certain limitations. The results presented in this study were based on 2D plane strain analysis, while the arteries are 3D structures. From the previous studies the absolute and peak

stresses were different for 2D and 3D simulations [47, 48]. Therefore, future research based on 3D geometry is required to better understand the fatigue behavior of the atherosclerotic plaque. The reconstructed geometry models were not at zero stress state because the obtained in vivo OCT data was already under the pressurized condition. Therefore, a shrink-stretch process was necessary to optimize the in vivo imaging data to the zero stress state model for the simulation, however, it is difficult to determine the shrinkage model using only in vivo data. From previous studies [49], an inner circumferential shrinkage of 7.9% was observed by comparing the in vivo / ex vivo MRI data. In order to compare the shrinkage and no- shrinkage models, one simulation has been done on the shrinkage model with a shrinkage rate of 7.9%. From the Fig. 10 (a) & (b), the maximum equivalent stresses were found at the same location for the no-shrinkage model and the shrinkage model with almost the same value. From the Fig 10 (c) & (d) the fatigue life has been slightly increased and the stress intensity factor has been slightly decreased by applying the shrinkage process. There was no significant difference between results from the shrinkage and no-shrinkage based simulations. An accurate shrinkage model is the challenge in obtaining the patient-specific shrinkage data from in vivo imaging. Besides, in this study, the shrinkage data from the literature is only suitable for the intima layer of the vessel. The patient-specific data sets which could determine the shrinkage of all the artery layers are required for more accurate simulations.

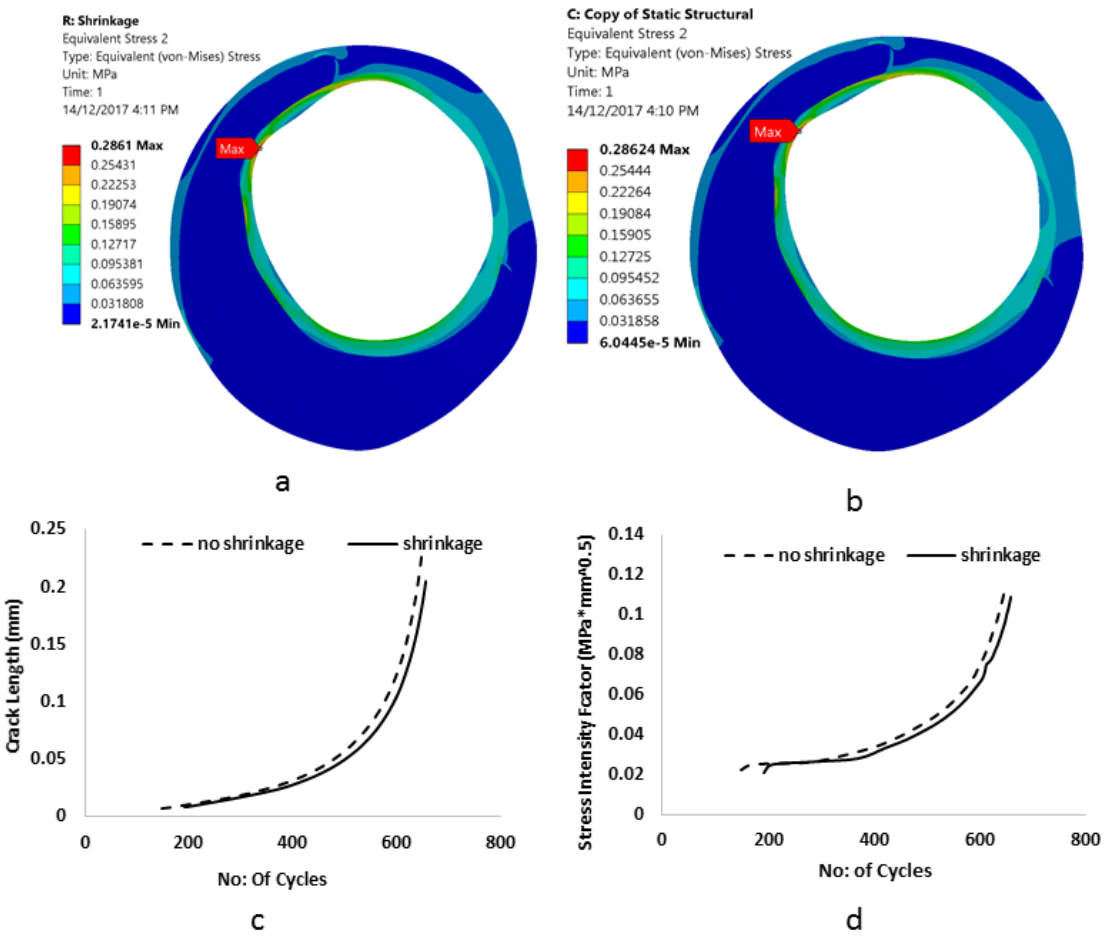

Fig. 10. Effect of Shrinkage, **a:** Maximum equivalent stress location-shrinkage model, **b:** Maximum equivalent stress location- no Shrinkage model, **c:** Variation of fatigue life for shrinkage and no shrinkage model, **d:** Variation of stress intensity factor for shrinkage and no shrinkage model

Moreover, since OCT has a low depth of penetration, the 3D reconstruction of an artery requires a combination of imaging techniques which is time consuming and costly and blood pressure has more impact that blood flow on the vessel wall. Therefore, a two-dimensional geometry, ignoring the effect of blood flow was considered for the fatigue crack growth modelling. Another limitation of this study was the use of simple isotropic material properties. This is due to the lack of appropriate experimental data for the fracture parameters. The Paris law constants were taken from the literature as the overall conclusions of the analysis would not have changed by considering different values. Also, the effect of initial crack length and the self-recovery ability of the living tissues were not considered. Moreover, relatively low number of reconstructed models were used in this

analysis. Due to the above mentioned limitations, the available data from the literature was used and the results were substantiated with the previous studies. Though these results may not be applicable to clinical outcomes in this current form, these findings provide valuable insight for future research and for designing therapies for clinical outcomes. In addition, more research is terms of patient specific XFEM based 3D fatigue crack growth simulations are needed to further validate and establish the clinical applications of the methodology. Also, to better improve the accuracy, efficiency and convergence of the models an adaptively refined XFEM [50] may be used in future studies. Future studies need to be focused on determining the c and m values for the Paris law including imaging the damage accumulation and failure [51] under the biomechanical environment.

5. CONCLUSION

In conclusion, atherosclerotic plaque rupture being the main cause of acute cardiovascular events and the factors involved in the initiation, progression and rupture are manifold. A novel framework, which can simulate the effects of cyclic loading and determine the fatigue crack growth rate was presented. In this study, the fatigue behavior of the OCT based patient-specific plaque models were analyzed using the XFEM based simulations. The results indicated that fatigue failure of the atherosclerotic plaque was mainly affected by the morphological features, constituents present and their spatial location with respect to each other. The present study also confirms previous findings and provides additional evidence with respect to crack initiation, propagation mechanism, and critical crack locations. We also found that the correlations between various morphological features such as local fibrous cap thickness, local lipid core thickness, lipid core area and calcification area can improve the ability to identify patients at highest risk when applied on large scale longitudinal studies. Therefore, future studies are required to better understand the fatigue failure of atherosclerotic plaque and establish the clinical applications of the methodology.

ACKNOWLEDGMENT

The authors would like to acknowledge the financial support of Queensland University of Technology (QUT) and as well as the technical support of high-performance computing and research support at QUT. This study was supported by ARC (FT140101152) and the PA Research Foundation (PARF). The authors would also like to acknowledge Sam Nardella from Leap Australia, Dr. Christopher Raffel from Prince Charles Hospital, Ms. Lee Jones and Ms. Parnia Zaki Khani from QUT for their insight and expertise that greatly assisted the research.

Conflict of interest statement

No conflicts of interest

REFERENCES

1. Nicholas M, et al., *Australian heart disease statistics 2015*. 2016, Melborne: National Feart Foundation of Australia.
2. Mozaffarian, D., et al., *Heart disease and stroke statistics-2016 update a report from the American Heart Association.* Circulation, 2016. **133**(4): p. e38-e48.
3. Benjamin, E.J., et al., *Heart Disease and Stroke Statistics—2017 Update: A Report From the American Heart Association.* Circulation, 2017.
4. Teng, Z., et al., *Coronary plaque structural stress is associated with plaque composition and subtype and higher in acute coronary syndrome the BEACON I (Biomechanical Evaluation of Atheromatous Coronary Arteries) study.* Circulation: Cardiovascular Imaging, 2014. **7**(3): p. 461-470.
5. Narula, J., et al., *Arithmetic of vulnerable plaques for noninvasive imaging.* Nature Clinical Practice Cardiovascular Medicine, 2008. **5**(SUPPL. 2).
6. Falk, E., *Pathogenesis of Atherosclerosis.* Journal of the American College of Cardiology, 2006. **47**(8 SUPPL.): p. C7-C12.
7. Davies, M.J. and A. Thomas, *Thrombosis and acute coronary-artery lesions in sudden cardiac ischemic death.* New England Journal of Medicine, 1984. **310**(18): p. 1137-1140.
8. Loree, H.M., et al., *Effects of fibrous cap thickness on peak circumferential stress in model atherosclerotic vessels.* Circulation Research, 1992. **71**(4): p. 850-858.
9. Finn, A.V., et al., *Concept of Vulnerable/Unstable Plaque.* Arteriosclerosis Thrombosis and Vascular Biology, 2010. **30**(7): p. 1282-1292.
10. Virmani, R., et al., *Lessons from sudden coronary death a comprehensive morphological classification scheme for atherosclerotic lesions.* Arteriosclerosis, thrombosis, and vascular biology, 2000. **20**(5): p. 1262-1275.
11. Yuan, C., *Carotid Atherosclerosis and Magnetic Resonance Imaging.* JACC: Cardiovascular Imaging, 2008. **1**(1): p. 58-60.
12. Glagov, S., et al., *Compensatory enlargement of human atherosclerotic coronary arteries.* New England Journal of Medicine, 1987. **316**(22): p. 1371-1375.
13. Tang, D., et al., *Cap inflammation leads to higher plaque cap strain and lower cap stress: An MRI-PET/CT-based FSI modeling approach.* Journal of Biomechanics, 2017. **50**: p. 121-129.
14. Guo, X., et al., *Quantify patient-specific coronary material property and its impact on stress/strain calculations using in vivo IVUS data and 3D FSI models: a pilot study.* Biomechanics and Modeling in Mechanobiology, 2017. **16**(1): p. 333-344.
15. Zahnd, G., et al., *Fusion of fibrous cap thickness and wall shear stress to assess plaque vulnerability in coronary arteries: a pilot study.* International Journal of Computer Assisted Radiology and Surgery, 2016: p. 1-12.
16. Tang, D., et al., *Image-based modeling for better understanding and assessment of atherosclerotic plaque progression and vulnerability: Data, modeling, validation, uncertainty and predictions.* Journal of Biomechanics, 2014. **47**(4): p. 834-846.
17. Tang, D., et al., *Local critical stress correlates better than global maximum stress with plaque morphological features linked to atherosclerotic plaque vulnerability: an in vivo multi-patient study.* BioMedical Engineering OnLine, 2009. **8**(1).
18. Li, Z.-Y., et al., *Stress analysis of carotid plaque rupture based on in vivo high resolution MRI.* Journal of Biomechanics, 2006. **39**(14): p. 2611-2622.

19. Li, Z.-Y., et al., *Structural analysis and magnetic resonance imaging predict plaque vulnerability: A study comparing symptomatic and asymptomatic individuals.* Journal of Vascular Surgery, 2007. **45**(4): p. 768-775.
20. Thondapu, V., et al., *Biomechanical stress in coronary atherosclerosis: emerging insights from computational modelling.* European heart journal, 2016: p. ehv689.
21. Brown, A.J., et al., *Role of biomechanical forces in the natural history of coronary atherosclerosis.* Nature Reviews Cardiology, 2016. **13**(4): p. 210-220.
22. Li, Z.-Y., et al., *How critical is fibrous cap thickness to carotid plaque stability?: A flow–plaque interaction model.* Stroke, 2006. **37**(5): p. 1195-1199.
23. Bank, A.J., et al., *Atherosclerotic plaque rupture: a fatigue process?* Medical Hypotheses, 2000. **55**(6): p. 480-484.
24. Pei, X., B. Wu, and Z.-Y. Li, *Fatigue Crack Propagation Analysis of Plaque Rupture.* Journal of Biomechanical Engineering-Transactions of the Asme, 2013. **135**(10).
25. Wu, B., X. Pei, and Z.-Y. Li, *How does calcification influence plaque vulnerability? Insights from fatigue analysis*, in *The Scientific World Journal*. 2014.
26. Pei, X., et al., *Fatigue Crack Growth Under Pulsatile Pressure and Plaque Rupture.* Jacc-Cardiovascular Imaging, 2014. **7**(7): p. 738-740.
27. Versluis, A., A.J. Bank, and W.H. Douglas, *Fatigue and plaque rupture in myocardial infarction.* Journal of Biomechanics, 2006. **39**(2): p. 339-347.
28. Huang, Y., et al., *In vivo MRI-based simulation of fatigue process: a possible trigger for human carotid atherosclerotic plaque rupture.* Biomedical Engineering Online, 2013. **12**.
29. Rezvani-Sharif, A., et al., *Stress analysis of fracture of atherosclerotic plaques: crack propagation modeling.* Medical & Biological Engineering & Computing, 2016: p. 1-12.
30. Prati, F., et al., *Expert review document on methodology, terminology, and clinical applications of optical coherence tomography: physical principles, methodology of image acquisition, and clinical application for assessment of coronary arteries and atherosclerosis.* European Heart Journal, 2009. **31**(4): p. 401-415.
31. Anderson, T.L. and T. Anderson, *Fracture mechanics: fundamentals and applications*. 2nd ed. 2005: CRC press.
32. Paris, P.C. and F. Erdogan. *A critical analysis of crack propagation laws*. 1963. ASME.
33. Erdogan, F. and G.C. Sih, *On the Crack Extension in Plates Under Plane Loading and Transverse Shear.* Journal of Basic Engineering, 1963. **85**(4): p. 519-525.
34. Khoei, A.R., *Extended finite element method: theory and applications*. 2014: John Wiley & Sons.
35. Belytschko, T. and T. Black, *Elastic crack growth in finite elements with minimal remeshing.* International journal for numerical methods in engineering, 1999. **45**(5): p. 601-620.
36. Melenk, J.M. and I. Babuška, *The partition of unity finite element method: basic theory and applications.* Computer methods in applied mechanics and engineering, 1996. **139**(1-4): p. 289-314.
37. Osher, S. and J.A. Sethian, *Fronts propagating with curvature-dependent speed: algorithms based on Hamilton-Jacobi formulations.* Journal of computational physics, 1988. **79**(1): p. 12-49.
38. Nijrolder, I., et al., *Fatigue in primary care: Longitudinal associations with pain.* PAIN, 2010. **150**(2): p. 351-357.
39. Bergara, A., et al., *Fatigue crack propagation in complex stress fields: Experiments and numerical simulations using the Extended Finite Element Method (XFEM).* International Journal of Fatigue, 2017. **103**: p. 112-121.

40. Broek, D., *Elementary engineering fracture mechanics*. 2012: Springer Science & Business Media.
41. Wang, L., et al., *Morphological and Stress Vulnerability Indices for Human Coronary Plaques and Their Correlations with Cap Thickness and Lipid Percent: An IVUS-Based Fluid-Structure Interaction Multi-patient Study.* Plos Computational Biology, 2015. **11**(12).
42. Cheng, G.C., et al., *Distribution of circumferential stress in ruptured and stable atherosclerotic lesions. A structural analysis with histopathological correlation.* Circulation, 1993. **87**(4): p. 1179-1187.
43. Morbiducci, U., et al., *Atherosclerosis at arterial bifurcations: evidence for the role of haemodynamics and geometry.* Thrombosis and Haemostasis, 2016. **115**(3): p. 484-492.
44. Finet, G., J. Ohayon, and G. Rioufol, *Biomechanical interaction between cap thickness, lipid core composition and blood pressure in vulnerable coronary plaque: impact on stability or instability.* Coronary artery disease, 2004. **15**(1): p. 13-20.
45. Gao, H. and Q. Long, *Effects of varied lipid core volume and fibrous cap thickness on stress distribution in carotid arterial plaques.* Journal of Biomechanics, 2008. **41**(14): p. 3053-3059.
46. Kiousis, D.E., et al., *A Methodology to Analyze Changes in Lipid Core and Calcification Onto Fibrous Cap Vulnerability: The Human Atherosclerotic Carotid Bifurcation as an Illustratory Example.* Journal of Biomechanical Engineering-Transactions of the Asme, 2009. **131**(12).
47. Balzani, D., et al., *Parallel simulation of patient-specific atherosclerotic arteries for the enhancement of intravascular ultrasound diagnostics.* Engineering Computations, 2012. **29**(8): p. 888-906.
48. Nieuwstadt, H.A., et al., *The influence of axial image resolution on atherosclerotic plaque stress computations.* Journal of Biomechanics, 2013. **46**(4): p. 689-695.
49. Huang, X., et al., *Patient-specific artery shrinkage and 3D zero-stress state in multi-component 3D FSI models for carotid atherosclerotic plaques based on in vivo MRI data.* Molecular & cellular biomechanics: MCB, 2009. **6**(2): p. 121.
50. Teng, Z.H., et al., *An adaptively refined XFEM with virtual node polygonal elements for dynamic crack problems.* Computational Mechanics, 2018.
51. Wu, S.C., T.Q. Xiao, and P.J. Withers, *The imaging of failure in structural materials by synchrotron radiation X-ray microtomography.* Engineering Fracture Mechanics, 2017. **182**: p. 127-156.